Isothermal Modeling of Gas Turbine Combustors: Computational Study

P. Koutmos* and J. J. McGuirk†
Imperial College of Science, Technology, and Medicine, London, England, United Kingdom

This paper is concerned with computations of a swirl-stabilized model tubo-annular combustor under isothermal conditions. The flow comprised a swirl-driven recirculation, two rows of radially injected jets, and an exit nozzle. The computations were based upon numerical solution of time-averaged transport equations for mass, momentum, turbulence energy, and dissipation using a finite-volume formulation. The combustor geometry was split into two zones, and the flow in the exit nozzle was computed using a general method for complex geometries. Laser-Doppler anemometry measurements of the velocity and turbulence fields were used to assess the performance of the numerical model. Predicted velocity distributions showed favorable agreement with measurements in the primary and intermediate zones although discrepancies increased in the dilution region. Predicted levels of turbulence energy were too low in regions of high anisotropy. A parametric study over the measured range of flow patterns indicated that local velocities were subject to errors of 30% in some small regions of the flow, but the mathematical model did simulate all observed trends. Further, it was demonstrated that, for isothermal flow, important global aspects of the flow (e.g., primary zone recirculation ratio) could be represented with acceptable accuracy for preliminary design purposes.

Nomenclature

$a,b,\ldots,m,n$	= measurement stations
$c_\mu, c_{\epsilon 1}, c_{\epsilon 2}$	= constants in k-ϵ turbulence model
D	= outer containing tube diameter
D_c	= internal combustor diameter
H	= exit nozzle height
k	= turbulence kinetic energy
$\dot{m}$	= mass flow rate
$\dot{m}_{pr}$	= primary jet mass flow rate
$\dot{m}_r$	= mass flow recirculating in primary zone
$\dot{m}_{sw}$	= swirler mass flow rate
P	= static pressure
$\dot{Q}$	= volumetric flow rate
$\dot{Q}_{annulus}$	= annulus volumetric flow rate, $\dot{Q}_{prim} + \dot{Q}_{sec}$
$\dot{Q}_{prim}$	= primary jets volumetric flow rate
$\dot{Q}_{sec}$	= secondary jets volumetric flow rate
$\dot{Q}_{sw}$	= swirler volumetric flow rate
r	= radial coordinate
$\bar{U},\bar{V},\bar{W}$	= mean velocities in Cartesian (x,y,z) or cylindrical polar coordinates (x,r,θ)
U_b	= bulk velocity inside the combustor
$\overline{u_i u_j}$	= Reynolds stress tensor
W	= exit nozzle width
x,y,z	= Cartesian coordinates
δ_{ij}	= Kronecker delta; 1 for $i=j$, 0 for $i\neq j$
ϵ	= turbulence energy dissipation rate
θ	= circumferential coordinate in cylindrical polar system
μ_t	= turbulent viscosity
ρ	= density
$\sigma_k, \sigma_\epsilon$	= constants in k-ϵ model

Subscripts

i,j	= indices of the tensorial notation
sw	= relating to swirler
pr	= relating to primary jets

Superscript

$\bar{}$	= time-averaged quantity

Introduction

IN recent years gas turbine combustor designs have placed heavy demands on liner temperature, exit temperature pattern factor, and low pollutant emission levels. Modern combustor designs should be able to achieve these stringent and sometimes conflicting requirements without compromising the durability of established designs, with acceptable development costs. It has also long been recognized that traditional design procedures are limited when significant jumps in technology are required; extrapolation from existing experience is then unreliable. Improved methods for combustor design can best serve the combustor engineer if they provide a better understanding of the fundamental processes occurring inside a combustor.

Computational fluid dynamics for combustor flows is being studied by all engine manufacturers.[1,2] The numerical models are continuously developed to increase confidence in their use as design and diagnostic tools. Because of the complexity of combustor flows, the route usually followed is to concentrate attention in validation studies on one or two of the components that comprise the overall combustor model. Perhaps most significantly this enables reliable model validation experiments to be conducted in simpler and better controlled flows.

Along these lines Sturgess and Syed,[3] Abujelala and Lilley,[4] and Sloan et al.[5] have concentrated on the prediction of confined axisymmetric swirling flows—an important constituent of many combustors. The preceding works highlighted the deficiencies of eddy viscosity models and recommended the use of higher-order turbulence models. Attention was also focused on the importance of the convection discretization scheme and the boundary conditions when direct comparison with measurement was attempted.

An additional feature of gas-turbine combustors is, however, the presence of rows of radially injected jets around the periphery. This creates regions of strong three-dimensionali-

Received April 29, 1989; revision received March 10, 1990.

*Research Assistant, Mechanical Engineering Department, Fluids Section; currently Lecturer, Department of Mechanical Engineering, University of Patras, Patras, Greece.

†Senior Lecturer, Mechanical Engineering Department, Fluids Section; currently Professor, Department of Transport Technology, University of Technology, Loughborough, Leicestershire, LE11 3TU, England, United Kingdom.

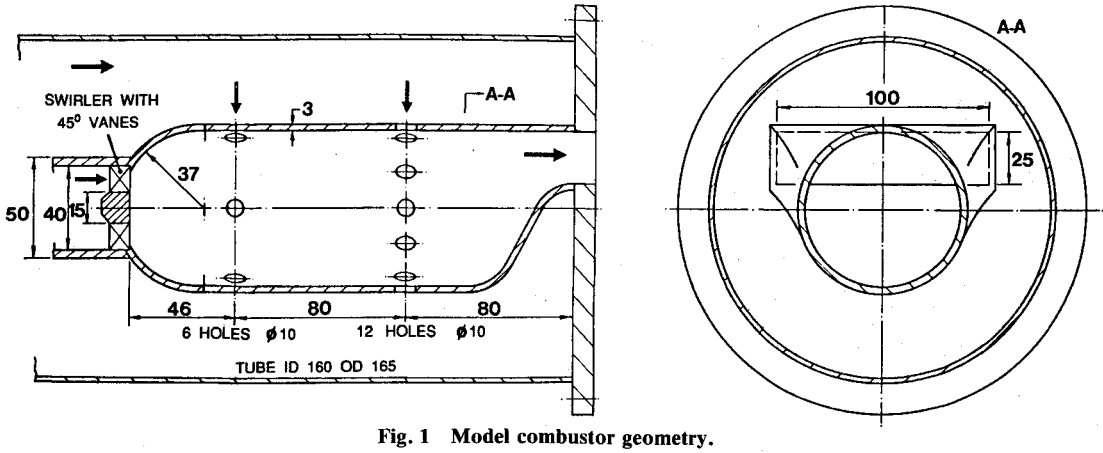

Fig. 1 Model combustor geometry.

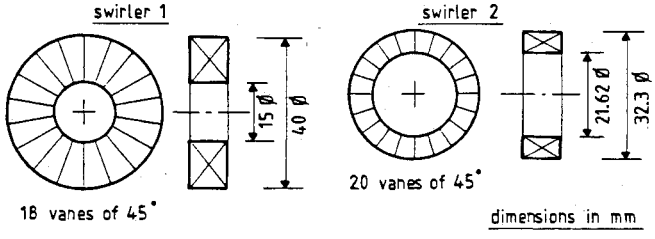

Fig. 2 Swirler geometry.

ties due to the discrete nature of the jets. The importance of the jet dilution process was investigated in Khan et al.,[6] Jones and McGuirk,[7] Chleboun et al.,[8] and Demuren.[9] Multiple-jet, multiple-row dilution systems have been modeled in Green and Whitelaw[10] in a water model of a simplified can type combustor, but without swirler. In this configuration detailed comparison between predictions and measurements showed only qualitative agreement. Wild et al.[11] modeled the flow inside a cylindrical combustor with three rows of holes and compared the performance of the k-ϵ eddy viscosity model against an algebraic stress model. Their experimental comparison did not demonstrate clearly the superiority of the latter and was hampered by the lack of experimental data.

Although jet-in-crossflow studies in isolation are useful, since modern combustors place the swirler and the first row of holes in close proximity, a strong interaction is likely. Jones and Priddin,[12] Swithenbank et al.,[13] and Jones and McGuirk[14] modeled the reacting flow inside cylindrical combustors with both swirler and radial jets. Uncertainty about the combustion model, limitations of computer storage, and paucity of measurements impaired assessment of the predictions. Production combustion systems have been modeled by Bruce et al.,[15] Coupland and Priddin,[1] and Burrus et al.[2] These works demonstrate the use of boundary conforming grid systems for handling the complex combustor wall shapes. However, the main problem in testing in such realistic combustor geometries is the lack of comprehensive benchmark type experimental data.

The main area of interest of the present work is the numerical investigation of the three-dimensional turbulence mixing processes induced inside a combustor by the close interaction of a swirler and two rows of jets. Since many aspects of reacting flows depend strongly on turbulence controlled mixing, isothermal flow studies are particularly convenient to avoid the complexities of variable density and reaction. The relevance to combustor model development is retained by using a model and a flow split that are in accord with practical experience. This places the emphasis in the current work on the ability of the turbulence model to simulate flow patterns that are representative of the aerodynamic behavior of practical combustion systems.

Flow Configuration

The geometrical configuration used for the present investigation is shown in Fig. 1; it represents a single can combustor from a tubo-annular type arrangement.[16] The perspex model is described in detail in Refs. 17 and 18. Two alternative swirlers were used (see Fig. 2). The vane geometry corresponded to a swirl number[19] of 0.75 for swirler 1 and 0.85 for swirler 2. Predictions were carried out for a variety of swirler flow rates (see Table 1) ranging from 10 to 35% of the total combustor volume flow rate.

Detailed measurements of the three mean velocity components and the corresponding turbulence intensities in the present geometry have been obtained with a laser-Doppler anemometer (see Koutmos and McGuirk[17,18]). In what follows the predicted results are compared in terms of contours based on measurements obtained on the network of measurement points of Fig. 3; this figure also shows the coordinate frame used to analyze the combustor. All contour levels are nondimensionalized by the bulk velocity in the combustor ($U_b = 4\dot{Q}_{\text{total}}/\pi D_c^2$, where D_c is the internal combustor diameter); the radial coordinate is scaled using D, the outer containing tube diameter.

Mathematical Model and Calculation Arrangements

The calculation of the flow inside the model combustor was achieved by solving the governing equations for steady, time-averaged, uniform property flow:

$$\frac{\partial}{\partial x_i}(\rho U_i) = 0$$

$$\frac{\partial}{\partial x_j}(\rho U_i U_j) = -\frac{\partial \bar{P}}{\partial x_i} - \frac{\partial}{\partial x_j}(\rho \overline{u_i u_j})$$

together with the equations corresponding to an eddy viscosity turbulence model closure. The turbulence model is the two equation k-ϵ model[20]

$$-\rho\overline{u_i u_j} = \mu_t\left[\frac{\partial U_i}{\partial x_j} + \frac{\partial U_j}{\partial x_i}\right] - \frac{2}{3}\delta_{ij}\rho k$$

Table 1 Combustor operating conditions in terms of flow splits[a]

$\dot{Q}_{\text{annulus}}$ ($m^3/s \times 10^{-4}$)	$\dot{Q}_{sw}/\dot{Q}_{tot}$ (%)	$\dot{Q}_{prim}/\dot{Q}_{sw}$	$\dot{Q}_{sec}/\dot{Q}_{prim}$
3.1	10	3.5	1.58
4.9	15	2.2	1.58
7.0	20	1.52	1.64
9.3	25	1.14	1.64
10.8	28	0.98	1.64
12.9	35	0.703	1.64

[a]($\dot{Q}_{\text{annulus}} = \dot{Q}_{\text{prim}} + \dot{Q}_{\text{sec}}$ held constant at 2.8×10^{-3} m^3/s, except for 35% case when $\dot{Q}_{\text{annulus}}$ was 2.045×10^{-3} m^3/s).

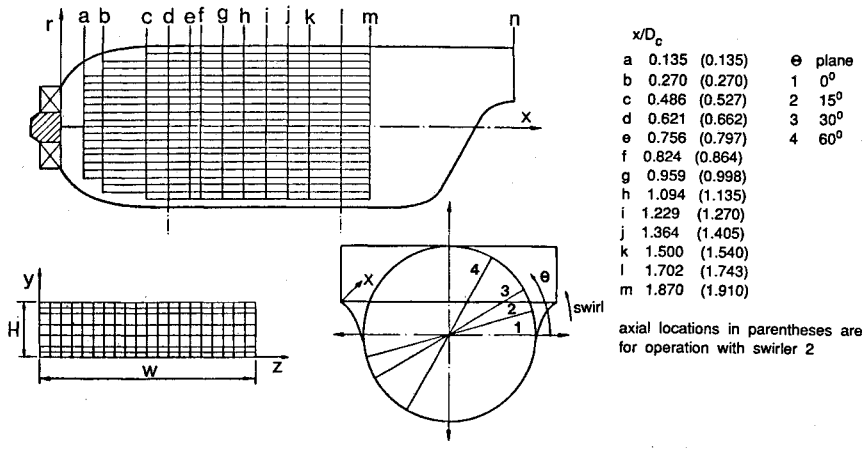

Fig. 3 Coordinate system and network of measurement points.

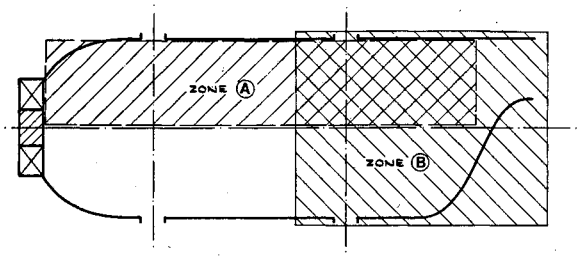

Fig. 4a Zonal division for combustor calculations.

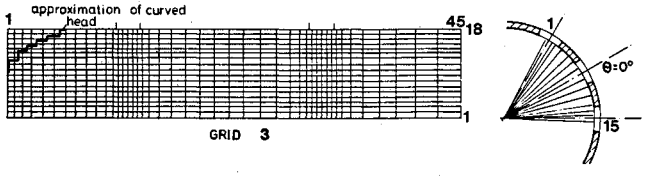

Fig. 4b Finite difference mesh used for zone A calculation.

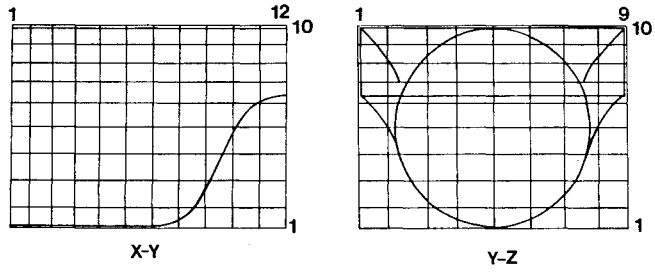

Fig. 5a Finite difference mesh used for zone B calculation.

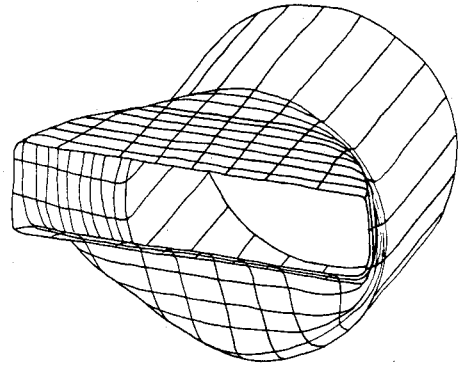

Fig. 5b Nozzle/can geometry for zone B calculation.

$$\mu_t = C_\mu \rho \frac{k^2}{\epsilon}$$

$$\frac{\partial}{\partial x_j}(\rho U_j k) = \frac{\partial}{\partial x_j}\left(\frac{\mu_t}{\sigma_k}\frac{\partial k}{\partial x_j}\right) - \rho\,\overline{u_i u_j}\frac{\partial U_i}{\partial x_j} - \rho\epsilon$$

$$\frac{\partial}{\partial x_j}(\rho U_j \epsilon) = \frac{\partial}{\partial x_j}\left(\frac{\mu_t}{\sigma_\epsilon}\frac{\partial c}{\partial x_j}\right) - C_{\epsilon 1}\frac{\epsilon}{k}\rho\,\overline{u_i u_j}\frac{\partial U_i}{\partial x_j} - C_{\epsilon 2}\,\rho\,\frac{\epsilon^2}{k}$$

with the constants $C_\mu = 0.09$, $C_{\epsilon 1} = 1.44$, $C_{\epsilon 2} = 1.92$, $\sigma_k = 1$, $\sigma_\epsilon = 1.3$.

These six equations were solved in finite-volume form using a computer program[7] for the calculation of jets in crossflow. The numerical formulation comprised a linearized, implicit, conservative scheme using hybrid differencing for the convection terms. The pressure velocity coupling was handled using the standard SIMPLE algorithm.[21] Log-law, equilibrium-based wall functions were used for near-wall nodes.[22]

The measurements[17,18] indicated a cyclic behavior over a 60-deg sector up to plane k just upstream of the secondary jet plane where asymmetries appeared due to the upstream effect of the nozzle. It was therefore possible to adopt a zonal approach where the whole combustor flow domain was split into two overlapping zones (Fig. 4a). Zone A comprised swirler, head, and both rows of holes, the cylindrical can geometry was artificially extended, and zero normal gradients were assigned at the domain end. Zone B included the exit nozzle and part of the upstream cylindrical barrel including the dilution holes. The flow in the nozzle was calculated with inlet conditions taken from zone A. This allowed a first assessment of the influence of the nozzle on the upstream flow. For the calculation of the flow in zone B, the numerical method described above was unaltered except that a rectangular Cartesian mesh was adopted. The complex combustor wall geometry within this grid was represented in a piecewise linear manner. Calculation of the intersection points of the surface of the nozzle (Fig. 5b) with the Cartesian grid lines (Fig. 5a) enabled identification of finite-volume cells, which were inside, completely outside, or internal but adjacent to the combustor wall. For cells intersected by the boundary, the intersection points were used to deduce a planar approximation to the wall boundary appropriate for that particular cell and to set up adjustments to the discretized equations for the distorted cell volume. Further details of the calculation arrangement can be found in Ref. 23.

The differencing scheme used in the calculation method is known to result in false diffusion errors. In addition, grid refinement difficulties were present due to limitations in available computer storage. However, the accuracy of the predictions was established by inspection of solutions obtained with successively refined meshes. Three meshes were used for the calculations: $18 \times 9 \times 9$ (grid 1), $34 \times 14 \times 12$ (grid 2), and $45 \times 18 \times 15$ (grid 3), grid nodes x, r, θ, respectively. Compar-

ison between solutions obtained with the two finer meshes were very similar (Fig. 6) and suggested that the finer mesh (Fig. 4b) was acceptable in terms of economy and accuracy. It would be preferable to use a higher-order convection discretization scheme, but in the present flow, the large generation of turbulence that occurs inside the combustor gives rise to high levels of eddy viscosity and consequently low values of cell Peclet numbers, such that, even on the relatively coarse meshes of grids 2 and 3, the first-order accurate scheme seems acceptable.

It should be emphasized that this grid refinement test also examined the significance of a progressively better representation of the curved combustor head using the castellated approximation inherent in the use of a simple rectangular mesh (Fig 4b). The near-wall profile at station c for the two finer meshes shows little change, implying that the details of how well the near-wall flow is resolved are not important in determining the overall flow pattern. This is well known for combustor flows since all combustors have near-wall film cooling flows whose details are important for the wall heat transfer, but which do not disturb the main internal flow structure, which is set up essentially by the swirler and jet flow interaction. This is why the current jagged mesh boundary treatment is acceptable, although a boundary conforming treatment would of course be preferable.

Only a very coarse Cartesian mesh of $12 \times 10 \times 9$ (x, y, z) grid nodes (Fig. 5a) was used to perform the calculation of zone B. The presence of large pressure gradients in the nozzle may be expected to dominate the flow and will reduce the sensitivity of the calculations to numerical diffusion errors, but finer grid calculations should be performed if the nozzle flow is to be studied in detail. In this case, a more correct zonal approach than that described above would redefine the interface between zone A and B as being just of one cell overlap and lying somewhere in the intermediate zone where upstream nozzle effects are weak. Then, an interaction between zone A and zone B calculations would be allowed by repeated passes through the system exchanging inlet/outlet boundary conditions between the two zones at the interface overlap. This approach has been successfully adopted in lobed mixer flow calculations by Koutmos and McGuirk.[24] This was not done in the present work since the main emphasis was laid on predictions in the primary zone (i.e., measurement planes a–g), where it was known from the measurements that even this more correct zonal approach would not have penetrated so far upstream. Our intention was only to provide a first estimate of the strength of the upstream nozzle effects on the secondary jet trajectories and, as seen below, for this the coarse mesh and cruder zonal approach were sufficient.

Boundary conditions for the calculation were taken as far as possible from the measurements. Cyclic boundary conditions were applied at the edges of the 60-deg calculation domain. At the swirler inlet uniform axial, azimuthal, and zero radial velocity profiles were specified, based on the mass flow rate and the swirl number. At the primary and secondary holes, the axial and azimuthal velocities were available from measurements[23] at the plane of the hole. The radial velocity was calculated from the mass flow rate appropriate to each hole. Profiles of the normal stresses were available immediately upstream of the swirler and in the plane of the holes; from these the turbulence kinetic energy boundary conditions were

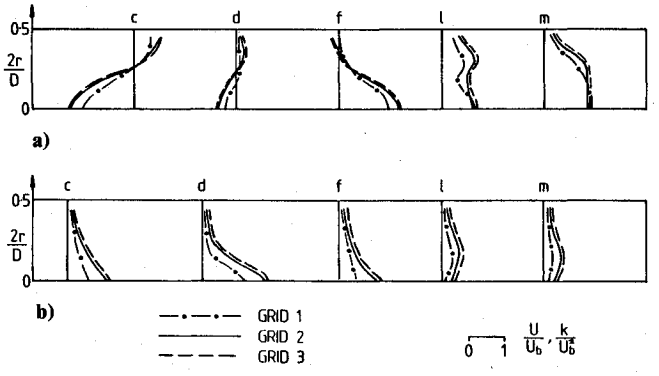

Fig. 6 Grid refinement tests, zone A calculation (θ = 0 deg, swirler 1, 15% swirler flow): a) axial velocity and b) turbulence kinetic energy.

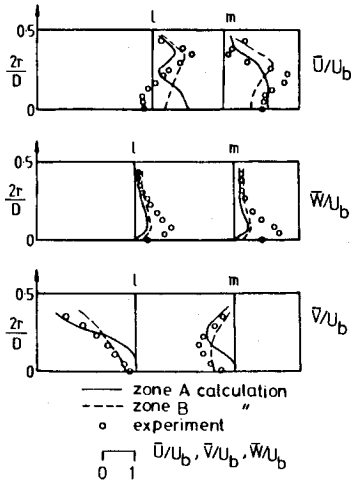

Fig. 7 Comparison of results of zone A and zone B calculations (station l and m, θ = 0 deg, swirler 1, 15% swirler flow).

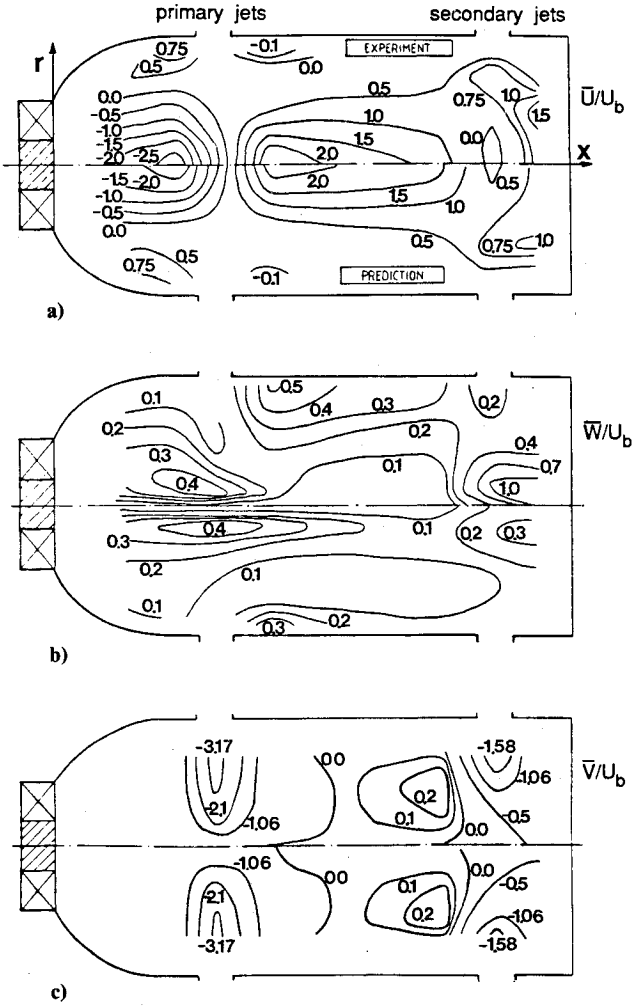

Fig. 8 Comparison of calculated and measured velocity fields for 10% swirler flow (θ = 0 deg, swirler 1): a) axial, b) azimuthal, and c) radial velocity.

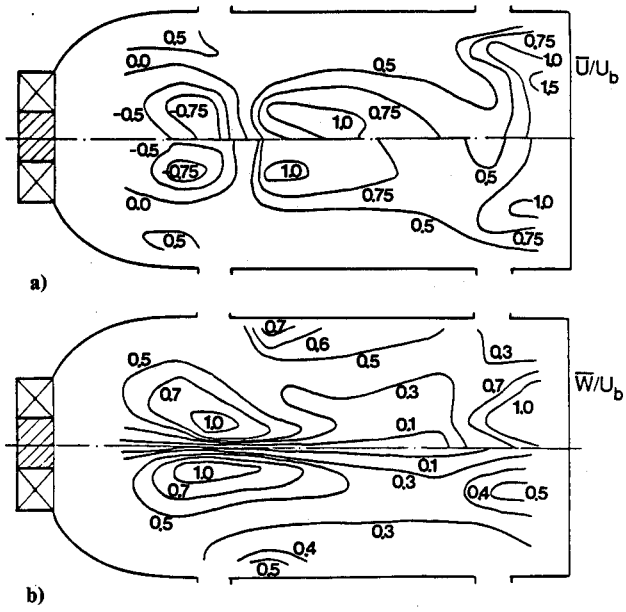

Fig. 9 Comparison of calculated and measured velocity fields for 20% swirler flow (θ = 0 deg, swirler 1): a) axial and b) azimuthal.

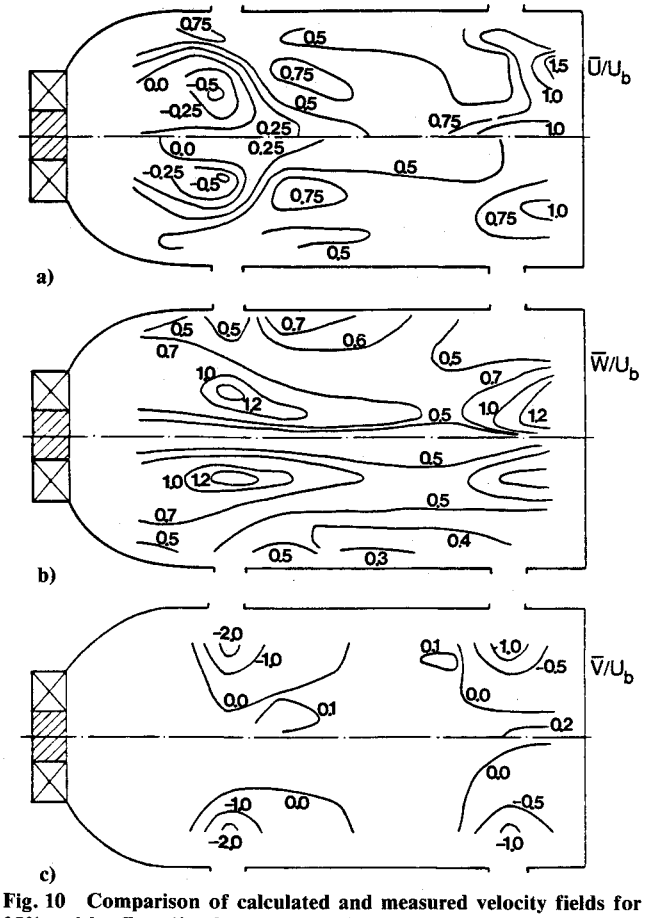

Fig. 10 Comparison of calculated and measured velocity fields for 25% swirler flow (θ = 0 deg swirler 1): a) axial, b) azimuthal, and c) radial velocity.

deduced. Boundary values for energy dissipation rate were calculated using a length scale proportional to the inlet port size.

Results

An overall evaluation of the correspondence between experiment and calculation as the swirler flow varies can be gained by comparing on the basis of contour plots (Figs. 8–11). In these the measured data are in the upper half, and calculations are in the lower half; the results of the zone B calculation have been included for the dilution zone. The extent of upstream interference induced by the nozzle is quantified in Fig. 7, which compares profiles for zone A and zone B calculations. A clear shift in the direction of the measurements is produced by taking the nozzle into account, although the predictions do not show as strong a tendency to backflow on the centerline at the secondary jet entry plane. The radial velocity profiles assume a much improved shape when nozzle effects are included.

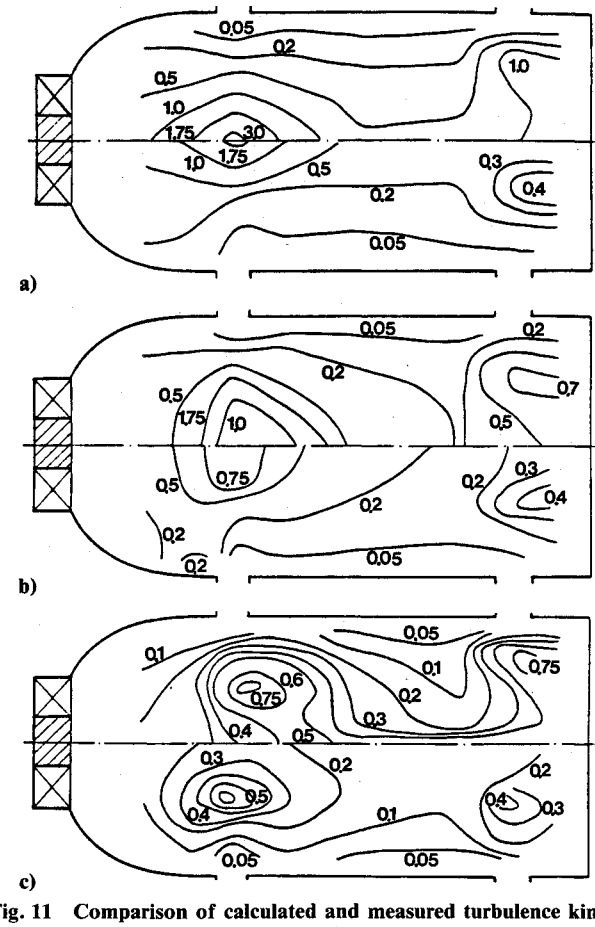

Fig. 11 Comparison of calculated and measured turbulence kinetic energy contours (θ = 0 deg, swirler 1): a) 10% swirler flow, b) 20% swirler flow, and c) 25% swirler flow.

At the lower swirler flow of 10% (Fig. 8), the steep penetration and dominance of the primary jets in creating the upstream recirculation is evident in both measurements and predictions. The length of the primary vortex is calculated correctly whereas its width is slightly underestimated (Fig. 8a). Negative axial velocities near the centerline were also underestimated with a maximum discrepancy of about 30% occurring. The predicted swirl velocity contours near the centerline (Fig. 8b) project deeper into the intermediate zone than the measured ones indicating that radial transfer of angular momentum is underpredicted in this region. As a result the free vortex type of profile seen in the measurements is not depicted clearly in the calculations apart from the region immediately downstream of the primary jets. For this swirler flow level, the location and spacing of the high radial velocity contours (Fig. 8c) implies that the lateral spread and depth of penetration of the primary jets is well predicted. Overall discrepancies are greater in the secondary jet centerline vicinity. This is the result of the inability of the model to predict the backflow near the combustor axis at this position as indicated in the axial velocity plots of Fig. 7 (plane l). Errors were generally smaller in other regions of the dilution zone.

A steep reduction in the primary vortex strength as the swirler flow level increases to 20% (Fig. 9a) is evident in both measurements and predictions. Similarly, the production of an off centerline peak in U in the intermediate zone is faithfully reproduced. The strength of the vortex is predicted well, but its size is again underestimated. Discrepancies in the swirl velocity contours (Fig. 9b) are if anything less than those found in the lower swirler flow level; a tendency to underpredict the high swirl momentum fluid entrained into the region behind the jets is observable although the presence of the fluid is well captured in the calculations.

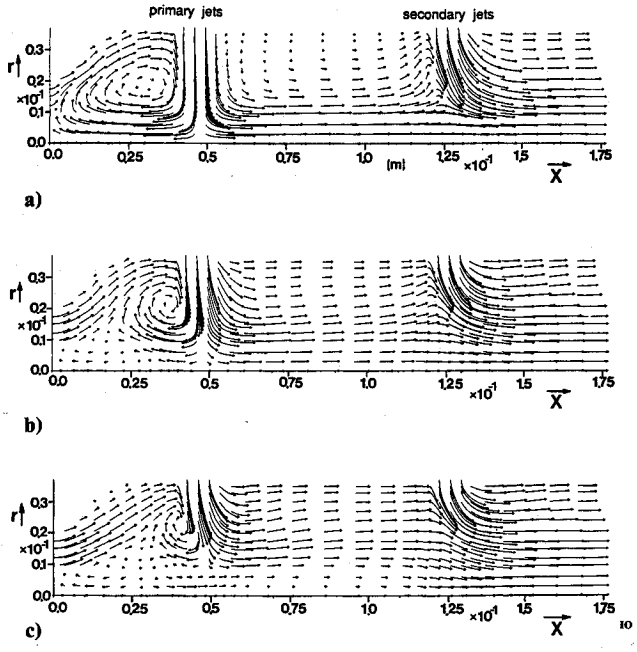

Fig. 12 Streakline plots of the velocity field ($\theta = 0$ deg, swirler 1; tracking time = 0.009 s): a) 10% swirler flow, b) 20% swirler flow, and c) 25% swirler flow.

Completely different primary zone patterns were observed in the experiments at 25% swirler flow. Figure 10 illustrates the degree to which the mathematical model mirrors this change. Comparison between Figs. 8a and 10a indicates that the decrease in primary vortex strength has been calculated with surprising accuracy; this can be attributed to an accurate prediction of primary jet penetration (Figs. 8c and 10c). The accuracy of predicting the swirl velocity field has also improved, and this can be related to an improved prediction of the turbulence field as discussed below. The presence of a core of strongly rotating fluid on the can centerline is a distinctive feature simulated well by the model.

Predicted and measured k fields for three swirler flow levels are depicted in Figs. 11a, 11b, and 11c. The contours illustrate that the spatial locations of intense turbulence generation are simulated well in both primary and dilution regions. Discrepancies may be found if we examine the levels of turbulence energy in these regions. In both lower swirler flows, the highest turbulence levels are found where jet impingement occurs, for both experiment and calculations. Unfortunately, the stronger the impingement the worse the agreement. At the lowest swirl level, the maximum value is underpredicted by almost a factor of 2; this error decreases to a factor of 1.3 for 20% swirler flow and to 1.2 for 25%. In the latter case, the movement in the position of maximum turbulence energy is well simulated.

The very high values of k found on the centerline under conditions of strong impingement are the result of anisotropy of the individual normal stresses (see Koutmos[23]). The turbulence energy for the lower swirler flow is dominated by the large values of $\sqrt{w^2}$ and $\sqrt{v^2}$ (up to 2.5 times $\sqrt{u^2}$, see Ref. 23). This high anisotropy may be interpreted as the result of large but very different production terms in the individual normal stress equations. On the centerline high values of $\partial U/\partial x$ and $\partial V/\partial r$ are found; by continuity these are related by $\partial U/\partial x = -2\partial V/\partial r = -2V/r$. Consequently, the production terms in the individual stress equations are of opposite sign (in $\overline{u^2}$: $-2\overline{u^2}\partial U/\partial x$ but in $\overline{v^2}$ and $\overline{w^2}$: $\overline{v^2}\partial U/\partial x$ and $\overline{w^2}\partial U/\partial x$, respectively). Similar behavior of the three normal stresses has been observed by Taylor and Whitelaw[25] at the rear stagnation point of a recirculation region behind a bluff body. It is probable that transport of each Reynolds stress component should receive separate consideration if correct partitioning of k is to be calculated for the near impingement regions. The underprediction of turbulence levels in this region (Fig. 11a) clearly confirms the weakness of the k-ϵ turbulence model, and this deficiency is likely to be responsible for the increased

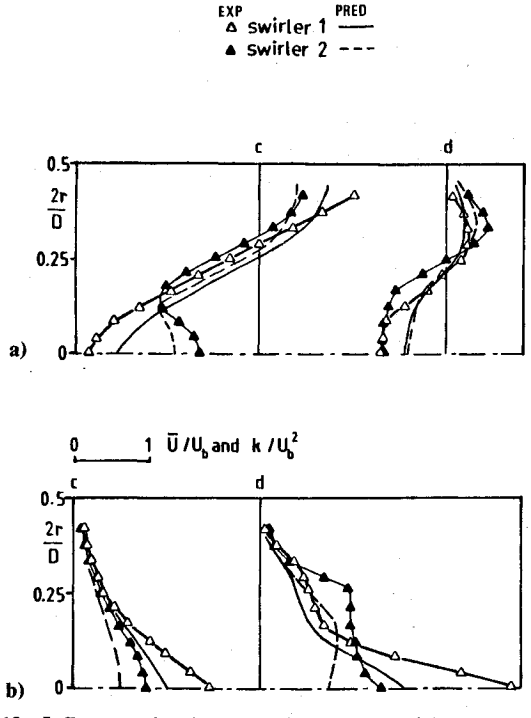

Fig. 13 Influence of swirler geometry on a) axial velocity profiles and b) turbulence kinetic energy ($\theta = 0$ deg, stations c and d, 15% swirler flow).

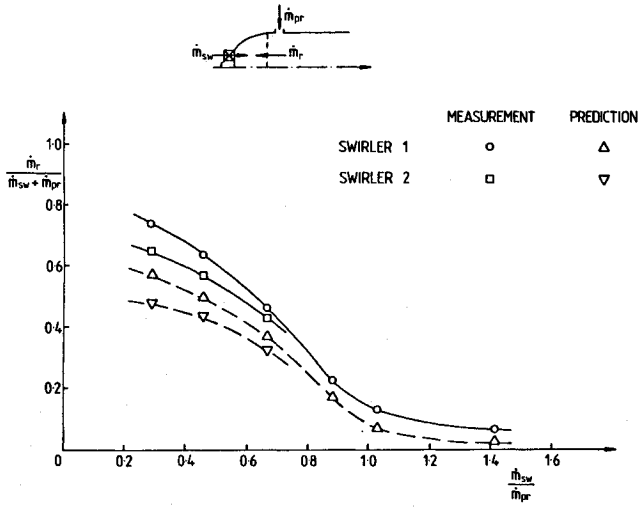

Fig. 14 Comparison of calculated and measured variation of the primary zone recirculation ratio.

discrepancy in the prediction of the axial and swirl components in the primary jet impingement region. Agreement improves in this region as the individual measured normal stresses become more uniform with increasing swirler flow (Fig. 11c).

An alternative method of illustrating the predicted internal flow pattern is to use a computational flow visualization by particle tracking. Figure 12 shows this gives an immediate picture of the features examined in detail in Figs. 8-10. Changes in primary jet penetration, collapse of the primary vortex, and a radial and axial shift of its "eye" all emerge clearly.

Finally, the ability of the model to calculate flow changes induced by a change in swirler is given in Fig. 13. A comparison between swirler 1 and swirler 2, both with 15% flow, is indicated. Swirler 2 (possessing a smaller outlet area and higher swirl number) weakened the primary zone recirculation (maximum negative axial velocity lower by 40%). Turbulence kinetic energy was also reduced by about 50%. The figure demonstrates that these variations were well reproduced by the calculations and predicted to within 25%.

Apart from the above detailed information, overall quantities of importance to design may be examined. One such parameter is the primary zone recirculation ratio (the amount of fluid entering through swirler and primary holes which participates in the primary vortex). Accurate information is lacking on recirculation ratios for primary zones, which utilize a combination of swirler and opposed jets.[16] In the present investigation, this quantity has been determined by integration of the negative part of the axial velocity profile at station c. Predicted values are compared with experiment in Fig. 14. Good qualitative similarity is exhibited over the entire range, which shows again the collapse of the primary vortex. Maximum discrepancies of about 17% are found at lower values of $\dot{m}_{sw}/\dot{m}_{pr}$, whereas a slight improvement is observed for the higher swirler flows; this is consistent with the detailed comparisons discussed above.

Concluding Remarks

The flow splits used in this investigation are typical of those encountered in traditional and current combustor designs,[1,26] and many features of the flow behavior obtained here are similar to those observed in rig testing of full-scale production chambers.[27] Consequently, the measured flow patterns are representative of the aerodynamic behavior of practical combustion systems and form an appropriate validation test case for combustor models.

Detailed comparison between calculation using a two-equation k-ϵ model and the experimental results showed that remarkably good agreement was obtained for the whole range of operating conditions. Quantitative discrepancies were highest in regions of strong jet-on-jet impingement where high anisotropy of the turbulence was identified. The k-ϵ turbulence model failed to predict accurately flow regions that were strongly anisotropic and possessed rapid spatial variations in the turbulence structure. The suspected importance of dominant generation due to normal stress/normal strain interaction suggested a clear cause of the failure of the eddy viscosity model. It may be observed that the flow whose turbulence structure is predicted best (25% swirler flow) is perhaps the least relevant to combustor design. Paradoxically, although the turbulence levels have large errors for the 10% swirler flow, the mean velocity field shows acceptable agreement with measurement (Fig. 8). This is no reason to be complacent about turbulence model errors, since these will show up much more in equations that are not dominated by the pressure gradients associated with impingement, as already observed in the swirl velocity comparisons.

Despite the above deficiencies, it has been shown here that the mathematical model is capable of predicting the effect of flow split variations and swirler geometry changes at a fairly detailed and quantitative level to a reasonable accuracy. Apart from this, overall quantities of importance to design such as an overall picture of the flow pattern and the primary zone recirculation can also be extracted conveniently from the model. It remains to be established whether this is also true for the scalar field and under variable density conditions.

Acknowledgments

The work reported here has been supported by the Ministry of Defence. The authors would like to acknowledge their gratitude for this support and the many useful discussions with staff at the Royal Aerospace Establishment (Pyestock), Rolls-Royce plc, and colleagues in both the Mechanical and Chemical Engineering Departments at Imperial College.

References

[1]Coupland, J., and Priddin, C. H., "Modelling the Flow and Combustion in a Production Gas Turbine Combustor," *Turbulent Shear Flows,* edited by L. A. Bradbury et al., Vol. 5, Springer-Verlag, 1987, pp. 310-323.

[2]Burrus, D. L., Shyy, W., and Braaten, M. E., "Numerical Models for Analytical Predictions of Combustor Aerothermal Performance Characteristics," AGARD-CP 422, Paper 25, 1987.

[3]Sturgess, G. J., and Syed, S. A., "Calculation of Confined Swirling Flows," AIAA Paper 85-0060, Jan. 1985.

[4]Abujelala, M. T., and Lilley, D. G., "Confined Swirling Flow Predictions," AIAA Paper 83-0316, 1983.

[5]Sloan, D. G., Smith, P. J., and Smooth, L. D., "Modelling of Swirl in Turbulent Flow Systems," *Progress in Energy and Combustion Science*, Vol. 12, 1986, pp. 163-250.

[6]Khan, Z. A., McGuirk, J. J., and Whitelaw, J. H., "A Row of Jets in a Cross-Flow," AGARD-CP 308, 1981.

[7]Jones, W. P., and McGuirk, J. J., "Computation of a Round Jet Discharging into a Confined Cross-Flow," *Turbulent Shear Flows 2,* edited by L. A. Bradbury et al., Vol. 2, Springer-Verlag, 1980, pp. 233-245.

[8]Chleboun, P. V., Craig, P. J., Sebbowa, F. B., and Sheppard, C. G. W., "A Study of Transverse Turbulent Jets in a Crossflow," *Combustion Science and Technology,* Vol. 29, 1982, pp. 107-111.

[9]Demuren, A. O., "Modelling Turbulent Jets in Crossflow," *Encyclopaedia of Fluid Mechanics,* edited by N. P. Cheremisinoff, Vol. 2, Gulf, New York, pp. 411-465.

[10]Green, A. S., and Whitelaw, J. H., "Isothermal Models of Gas Turbine Combustors," *Journals of Fluid Mechanics,* Vol. 126, 1983, pp. 399-412.

[11]Wild, P. N., Boysan, F., Swithenbank, J., and Lu, X., "Three-Dimensional Gas Turbine Combustor Modelling," AGARD-CP 422, Paper 27, 1987.

[12]Jones, W. P., and Priddin, C. H., "Predictions of the Flow Field and Local Gas Composition in Gas Turbine Combustors," *Proceedings of the 17th International Symposium on Combustion,* 1978, pp. 399-409.

[13]Swithenbank, J., Turan, A., and Felton, P. G., "Three-dimensional Two-Phase Modelling of Gas-Turbine Combustors," *Gas Turbine Combustor Problems,* edited by A. H. Lefebvre, Hemisphere, Washington, DC, 1978, pp. 249-314.

[14]Jones, W. P., and McGuirk, J. J., "Mathematical Modelling of Gas Turbine Combustion Chambers," AGARD-CP 275, Paper 4, 1980.

[15]Bruce, T. W., Mongia, H. C., and Reynolds, R. S., "Combustor Design Criteria Validation," USARTL TR-78-55, Vols. 1-3, 1979.

[16]Lefebvre, A. H., *Gas Turbine Combustion,* Hemisphere, Washington, DC, 1983.

[17]Koutmos, P., and McGuirk, J. J., "Investigation of Swirler/Dilution Jet Flow Split on Primary Zone Flow Patterns in a Water Model Can Type Combustor," *Journal of Engineering for Gas Turbines and Power (ASME),* Vol. 111, 1989, p. 310.

[18]Koutmos, P., and McGuirk, J. J., "Isothermal Flow in a Gas Turbine Combustor: A Benchmark Experimental Study," *Experiments in Fluids*, Vol. 7, 1989, p. 344.

[19]Beer, J. M., and Chigier, N. A., *Combustion Aerodynamics,* Applied Science, London, 1972.

[20]Jones, W. P., and Launder, B. E., "Prediction of Low Reynolds Number Phenomena with a Two Equation Model of Turbulence," *International Journal of Heat and Mass Transfer,* Vol. 16, 1973, p. 1189.

[21]Patankar, S. V., *Numerical Heat Transfer and Fluid Flow,* Hemisphere, Washington, DC, 1981.

[22]Launder, B. E., and Spalding, D. B., "The Numerical Computation of Turbulent Flow," *Computer Methods in Applied Mechanics and Engineering,* Vol. 3, 1974, pp. 269–289.

[23]Koutmos, P., "An Isothermal Study of Gas Turbine Combustor Flows," Ph.D. Dissertation, Univ. of London, London, 1985.

[24]Koutmos, P., and McGuirk, J. J., "Turbofan Forced Mixer/Nozzle Temperature and Flow Field Modelling," *International Journal of Heat and Mass Transfer*, Vol. 32, 1989, p. 1141.

[25]Taylor, A., and Whitelaw, J. H., "Velocity Characteristics in the Turbulent Near Wakes of Confined Axisymmetric Bluff Bodies," *Journal of Fluid Mechanics,* Vol. 139, 1984, p. 391.

[26]Bhangu, J. K., Snape, D. M., and Eardley, B. R., "The Design and Development of a Low Emissions Transply Combustor for the Civil Spey Engine," AGARD-CP 353, 1983.

[27]Gradon, K., and Miller, S. C., "Combustion Development on the Rolls-Royce Spey Engine," *Combustion in Advanced Gas Turbine Systems,* edited by I. E. Smith, Vol. 10, Cranfield International Symposium Series, Pergamon, 1968.